Optical properties of tilted II-VI superlattices grown on vicinal surfaces

L. Marsal,* A. Wasiela, G. Fishman,† and H. Mariette
Laboratoire de Spectrométrie Physique, Université J. Fourier, Grenoble I, CNRS (UMR 5588), Boîte Postale 87, F-38402 Saint Martin d'Hères Cédex, France

F. Michelini
INSA–Laboratoire de Physique de la Matière Condensée de Toulouse–CNRS (UMR 5830), Département de Génie Physique, 135, Avenue de Rangueil, F-31077 Toulouse Cédex 04, France

S. Nagahara and T. Kita
Department of Electrical and Electronics Engineering, Faculty of Engineering, Kobe University, Rokkodai 1-1, Nada, Kobe 657-8501, Japan

(Received 26 May 2000; revised manuscript received 27 October 2000; published 2 April 2001)

We have investigated the lowest emission state in tilted superlattices as a function of their tilt angle. The II-VI tilted superlattices, $CdTe/Cd_xMg_{1-x}Te$ and $CdTe/Cd_xMn_{1-x}Te$, were obtained by molecular beam epitaxy on vicinal substrates misoriented by 1°, which corresponds to a 186-Å terrace width. The tilt sensitivity of the optical properties is shown by both theoretical calculations and experimental results. The one-dimensional character is studied experimentally by optical spectroscopy in both excitation regimes: continuous wave and time-resolved spectroscopy. In continuous-wave photoluminescence spectra, an energy redshift of about 15 meV is observed when the superlattice is vertical. Such behavior is accounted for quantitatively by a theoretical approach that uses a periodic modulation potential to describe the lateral confinement and that takes into account the intermixing between Cd atoms and Mn (Mg) ones. In time-resolved spectroscopy, a temperature dependence of the decay time that is typical of exciton thermalization in one-dimensional systems is observed. Both these results, the energy shift and the lifetime dependence, are very sensitive to the one-dimensional character, that is, to the tilt angle of the tilted superlattice, as calculated theoretically.

DOI: 10.1103/PhysRevB.63.165304 PACS number(s): 73.21.−b, 81.15.Hi, 78.55.Et, 78.20.Bh

I. INTRODUCTION

Organized growth of semiconductors on vicinal surfaces is an attractive way to realize one-dimensional quantum structures in a single technological step. The advantage of this approach is that the array of quantum wires, also called a lateral or tilted superlattice, can have a period on the 10-nm scale with a lateral confinement potential that depends on the degree of modulation of the lateral composition. The repeated deposition of a fractional monolayer m of material A followed by a fractional monolayer n of material B results in a tilted A_mB_n superlattice (TSL). TSL's of III-V compounds have been reported extensively (see, for example, Refs. 1–5), and more recently TSL's of II-VI compounds have been grown by atomic layer epitaxy.[6] Practically, one of the main challenges is the precise control of the impinging atomic fluxes, to get a surface coverage $p=m+n$ as close as possible to unity, for which the TSL is vertical; any departure ε from p equal to unity ($p=1+\varepsilon$) leads to a severe tilt of the TSL with respect to the [001] growth direction. The present paper deals with this problem, namely, the strong dependence of the electronic properties of II-VI TSL structures on ε, presenting both theoretical and experimental (optical) results.

As concerns the optical measurements, we will focus on the problem of photoluminescence (PL) dynamics in quantum wires (QWR's). In particular, we report measurements of PL decay times and their temperature dependence in nanometer-scale QWR's, and compare these results with those obtained for quantum wells (QW's). The radiative lifetime of excitons confined in ideal quantum wires has been predicted[7] to be one order of magnitude higher than that of excitons confined in QW's.[8] These theoretical predictions assume that excitons are free to move in the unconfined direction so that only excitons with a center-of-mass wave vector smaller than k_0 (where k_0 is the wave vector of a photon having the same energy as the $k=0$ exciton) can decay radiatively with conservation of energy momentum. In real heterostructures, however, it is difficult to observe this intrinsic radiative lifetime directly due to localization of the excitons, which is induced by potential fluctuation, always present in the quantum heterostructures.[9] Evaluation of the intrinsic radiative lifetime in nanostructures relies on measurement of the temperature dependence of the decay time.

In QW structures, a linear increase of the effective lifetime with temperature has been predicted[8,10] for a two-dimensional (2D) exciton, with a slope proportional to the intrinsic radiative lifetime. This is due to the thermal distribution of the exciton population: when the temperature increases, the fraction of excitons that participate in radiative decay (that is, those with a wave vector smaller than k_0) decreases, and so the effective lifetime is longer than the radiative one and has a linear temperature dependence.

As concerns the QWR's, a similar calculation was performed by Citrin [7] who predicted that the effective lifetime would vary as the square root of temperature due to the different densities of states in a one-dimensional system. Previous experiments on V-groove GaAs QWR's (Ref. 9) and on

cleaved-edge-overgrown GaAs QWR's (Ref. 11) estimate the intrinsic radiative lifetimes from this temperature dependence. The time-resolved spectroscopy data reported here as a function of temperature show such 1D behavior in II-VI TSL structures.

The paper is organized as follows.

We first present a theoretical approach that allows us to describe the electronic properties of the TSL system as a function of the tilt angle. This theoretical calculation is based on a previous theoretical model developed by Mélin and co-workers[12] for GaAs/$Ga_xAl_{1-x}As$ TSL systems. In the present case, for II-VI TSL systems, the modulation potential that describes the lateral confinement is of the same order of magnitude as the kinetic energies of both electrons and holes. As a consequence, a complete calculation (using a wide basis) of the energy states and the wave functions of the electrons and holes in the TSL is presented in detail.

In the second part, the procedure for growing II-VI TSL's, in two types of materials systems, CdTe/$Cd_xMn_{1-x}Te$ and CdTe/$Cd_xMg_{1-x}Te$, is described in detail. These TSL's are characterized by their cw photoluminescence spectra: the energy redshift observed for the excitonic emission is related to the tilt angle of the TSL, and is compared to the theoretical calculation. This allows us to confirm the 1D character of the appropriate part of the selected area of the sample, and to study the limitations of the lateral confinement due to some intermixing between Cd and Mn (or Cd and Mg).

Finally, a systematic study of the decay time versus temperature is performed by time-resolved spectroscopy for both the QW and the TSL excitonic emissions. When the TSL is vertical, the PL decay times in the TSL were found to vary less with increasing temperature than those of the reference QW; moreover, the decay time dependence is roughly proportional to the square root of temperature. Such a temperature behavior of the lifetime is an unambiguous signature of a 1D system and allows us to show that the *intrinsic* radiative lifetime is two orders of magnitude larger in the QWR than in the QW.

II. THEORETICAL APPROACH

A. Modeling of the tilted superlattice

The TSL heterostructures consist of arrays of CdTe/$Cd_{0.76}Mn_{0.24}Te$ quantum wires stacked in the x direction and parallel to the [010] crystallographic orientation; the whole structure is embedded in $Cd_{0.74}Mg_{0.26}Te$ barriers along the y growth direction parallel to [001] [see Fig. 1(a) for a complete sketch of the TSL]. Instead of the expected abrupt modulation between pure CdTe and $Cd_{0.76}Mn_{0.24}Te$, we get something close to a sinusoidal modulation between $Cd_{0.92}Mn_{0.08}Te$ and $Cd_{0.84}Mn_{0.16}Te$ compositions: it enables us to take into account the intermixing of Cd and Mn, which occurs during the epitaxy, as studied before.[13,14] This intermixing model, which is discussed in Sec. III B, leads to Mn compositions in the middle of the wire and the middle of the barrier of 8% and 16%, respectively. The lateral confinement inside the TSL is well described by a sinusoidal modulation potential:

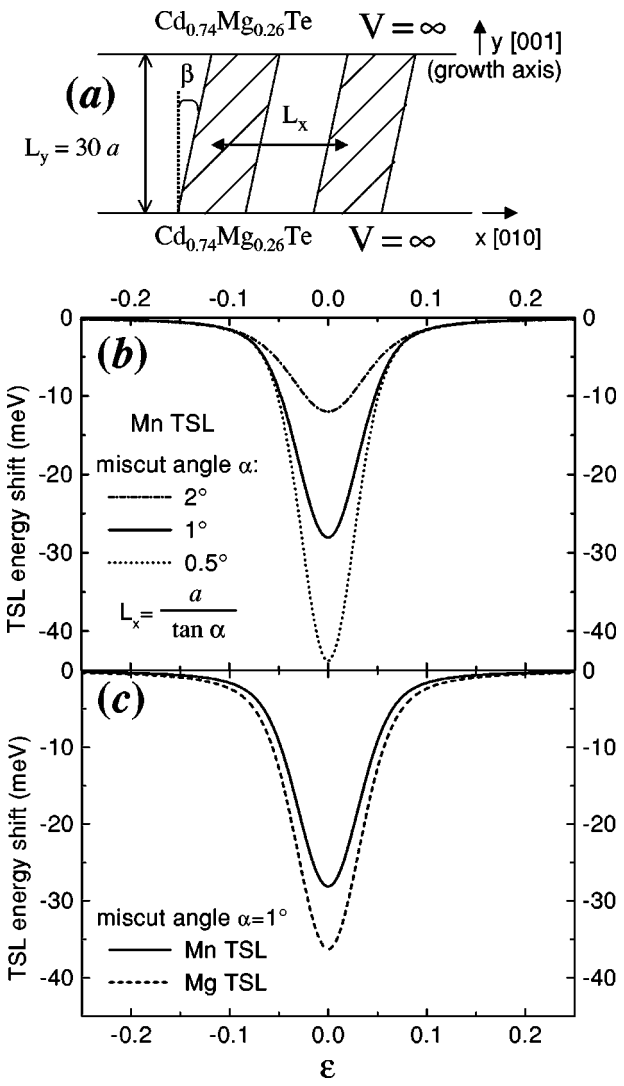

FIG. 1. (a) Sketch of the tilted superlattice with all the parameters used for our calculation; the lateral confinement in the x direction arises from the modulation potential $V(x,y)$ (see text); the tilt angle β is given by $\tan\beta=\varepsilon L_x/a$; (b) Calculated energy shift for a CdTe/$Cd_{0.76}Mn_{0.24}Te$ superlattice versus ε, and for three different misorientations α: 2°, 1°, and 0.5°, corresponding to terrace widths of, respectively, 93 Å, 186 Å, and 371 Å; (c) calculated energy shift for a 1° misorientation versus ε, and for two different compositions: a CdTe/$Cd_{0.76}Mn_{0.24}Te$ superlattice, and a CdTe/$Cd_{0.74}Mg_{0.26}Te$ superlattice.

$$V_N(x,y)=V_{Nmod}\cos(2\pi x/L_x-2\pi\varepsilon y/a), \qquad (2.1)$$

where ε is the tilt parameter as previously defined, L_x the terrace width, $a=3.24$ Å is the step height of the vicinal substrate, and $N=C$ or V for the conduction or the valence band, respectively. We also introduce the tilt angle β that is simply given by $\tan\beta=\varepsilon L_x/a$. The numerical values of V_{Nmod} corresponding to a CdTe/$Cd_xMn_{1-x}Te$ superlattice (Mn TSL) are the following: $V_{Cmod}=42.5$ meV and $V_{Vmod}=21.25$ meV. The potential expression (2.1) includes a ''classical'' part $2\pi x/L_x$ that takes into account the wire periodicity along the x direction, but also a contribution $2\pi\varepsilon y/a$ that enables us to deal with the superlattice tilt. In

the growth direction (y), the potential $V'_N(y)$ is due to the $Cd_{0.74}Mg_{0.26}Te$ barriers, i.e., $V'_N(y)=0$ inside the TSL width ($0<y<L_y$), and $V'_N(y)=V'_{Nout}$ in the barriers. Initially, we will consider the barriers in the y direction as infinite, i.e., we take $V'_{Nout}=\infty (N=C \text{ or } V)$; this approximation will be discussed at the end of Sec. II C. Finally, no strain effects are included because the $Cd_{0.74}Mg_{0.26}Te$ barriers match the $Cd_{0.96}Zn_{0.04}Te$ substrate and the mean composition of the TSL, $Cd_{0.88}Mn_{0.12}Te$, gives a strain of 0.03%, which is negligible given the other uncertainties.

We calculated the confinement energies and the associated envelope functions in both the conduction and the valence band for different values of ε between -1 and $+1$, for a given miscut angle α, i.e., for a given terrace width L_x. Since our goal is to compare the properties of the TSL for different values of ε, and assuming that the exciton-binding energy does not vary much in the considered ε range,[12] we will not take it into account. Before describing the general calculation, we first focus on particular cases, corresponding to large tilt angles ($\beta \geqslant 89°$, i.e., $|\varepsilon| \geqslant 1$) and perfect vertical superlattices ($\beta=0$, i.e., $\varepsilon=0$).

Finally, this calculation is also applied to Mg TSL's, with the following potential values corresponding to arrays of intended composition $CdTe/Cd_{0.74}Mg_{0.26}Te$: $V_{Cmod}=46.2$ meV and $V_{Vmod}=23.1$ meV.

B. Limiting cases

1. Case of the large tilt angles β

Let us consider a 1° misoriented surface, and a tilt corresponding to $\varepsilon=0.1$. This gives a tilt angle β of around 80°. Therefore, we shall consider that for values of $|\varepsilon| \geqslant 1$ (i.e., $\beta \geqslant 89°$), there is no longer a superlattice but a simple quantum well having the mean composition (here $Cd_{0.88}Mn_{0.12}Te$). In this case, we treat the heterostructure as a $Cd_{0.88}Mn_{0.12}Te$ quantum well with infinite barriers. The calculation is therefore analytical, and the resulting confinement energy gives a reference for the subsequent calculations.

2. Vertical superlattice: $\varepsilon=0$

For zero tilt angle, the heterostructure corresponds to a perfect vertical superlattice. In this particular case, the modulation potential $V_N(x,y)$ no longer depends on y, and is simply $V_N(x)$. The confinements in the x and y directions can be separated. In the growth direction (y), the confinement is associated with a $Cd_{0.92}Mn_{0.08}Te$ quantum well, embedded in $Cd_{0.74}Mg_{0.26}Te$ barriers considered as infinite (see end of Sec. II C). In the lateral direction (x), the confinement potential is $V_N(x)=V_{Nmod}\cos(2\pi x/L_x)$. Assuming a parabolic approximation for both the conduction and the valence band dispersions, the Schrödinger equation for the x-direction motion is the following:

$$-\frac{\hbar^2}{2m_N}\frac{d^2\varphi}{dx^2}+V_{Nmod}\cos(2\pi x/L_x)\varphi=e\varphi, \qquad (2.2)$$

with $m_c=0.096m_0$ and $m_v=0.6m_0$ (heavy-hole mass). This equation can be rewritten, with $v=\pi x/L_x$, as

$$\frac{d^2\varphi}{dv^2}+[a-2q\cos(2v)]\varphi=0 \qquad (2.3)$$

with $a=e/E_{Nc}$ and $q=V_{Nmod}/(2E_{Nc})$. E_{Nc} is the kinetic energy of the particle for $k_x=\pi/L_x$, i.e., $E_{Nc}=\hbar^2/2m_N(\pi/L_x)^2$. Equation (2.3) corresponds exactly to Mathieu's equation:[15] we are then able to calculate the energies e of the TSL and its wave functions φ along the x axis. With the numerical values given above (i.e., for a Mn TSL on a 1 °C substrate), the total confinement (conduction + valence band) obtained in the wires induces an energy redshift of 27 meV. Here the reference for the redshift is the quantum well of $Cd_{0.88}Mn_{0.12}Te$, i.e., the situation for large values of ε (see Sec. II B 1). Thus, a redshift is expected for the luminescence peak of the TSL when going from a tilted superlattice to a vertical one.

C. Numerical calculations in the general case

We obtained the ground-state energy and envelope functions of the TSL numerically using the Luttinger formalism. The calculation cannot be simplified here as it was done in the case of $GaAs/Ga_xAl_{1-x}As$ TSL's (see Ref. 12). Indeed, in the latter case, the coupling induced by the modulation potential was restricted to three k_x states, namely, $k_x=0$ and $k_x=\pm 2\pi/L_x$. This was justified by the smaller values of V_{Nmod} as compared with the ones of the kinetic energies E_{Nc} of both electrons and holes, especially when $k_x>2\pi/L_x$. For $GaAs/Ga_xAl_{1-x}As$ TSL's, these values are typically:

$$\frac{V_{Cmod}/2}{E_{c\frac{2\pi}{L_x}}}\approx 0.3-0.4 \quad \text{and} \quad \frac{V_{Cmod}/2}{E_{c\frac{4\pi}{L_x}}}\approx 0.1$$

for the conduction band,

$$\frac{V_{Vmod}/2}{E_{c\frac{2\pi}{L_x}}}\approx 0.4-0.6 \quad \text{and} \quad \frac{V_{Vmod}/2}{E_{c\frac{4\pi}{L_x}}}\approx 0.15-0.2$$

for the valence band.

By contrast, these ratios are completely different for our CdTe/Cd(Mn,Mg)Te TSL's, where

$$\frac{V_{Cmod}/2}{E_{c\frac{2\pi}{L_x}}}\approx 0.4-0.5 \quad \text{and} \quad \frac{V_{Cmod}/2}{E_{c\frac{4\pi}{L_x}}}\approx 0.1-0.2$$

for the conduction band,

$$\frac{V_{Vmod}/2}{E_{c\frac{2\pi}{L_x}}}\approx 3.2-3.3 \quad \text{and} \quad \frac{V_{Vmod}/2}{E_{c\frac{4\pi}{L_x}}}\approx 0.8-0.9$$

for the valence band.

This is due to the larger modulation potential present in our samples and the smaller kinetic energies due to the heavier effective masses in II-VI as compared to III-V semiconductors. Thus in the present case, the calculation with three coupling states is not justified anymore, especially for the valence band. We consider here a complete calculation for which a wide basis was used, not only along the x direction (lateral modulation), but also along the y direction (growth axis).

Our calculation is an extension of a calculation done for isolated quantum-wire heterostructures.[16] In the present case, the effective-mass Hamiltonian is projected on a Fourier basis that allows us to deal with the periodic part of the $V_N(x,y)$ modulation potential. The basis envelope functions are then

$$|kn\rangle|n'\rangle = \left| \frac{1}{\sqrt{L_x}} \exp i\left[k_x + n\left(\frac{2\pi}{L_x}\right)\right] x \right\rangle \left| \sqrt{\frac{2}{L_y}} \sin\left(\frac{n'\pi y}{L_y}\right)\right\rangle. \tag{2.4}$$

The envelope functions and the associated confinement energies are determined for a zero wave vector **k** [where **k** is parallel to the direction of the wires (z), which is the spin quantization axis as well]. The conduction band is treated as a parabolic band near the minimum, and the topmost valence band is described by the Luttinger-Kohn Hamiltonian. Thus, the conduction-band Hamiltonian is written $\mathcal{H}_C = (p_x^2 + p_y^2)/2m_c + V_C(x,y) + V'_C(y)$, where m_c is the electron effective mass, $m_c = 0.096 m_0$. The valence-band Hamiltonian is written: $\mathcal{H}_V = \mathcal{H}_{LK} + V_V(x,y) + V'_V(y)$, where $\mathcal{H}_{LK}$ is the Luttinger-Kohn Hamiltonian. With $k_z = 0$, $\mathcal{H}_{LK}$ is reduced to a 2×2 matrix in the basis $|3/2 \pm 3/2\rangle$, $|3/2 \mp 1/2\rangle$:

$$\mathcal{H}_{LK} = \left(-\frac{\hbar^2}{2m_0}\right) \begin{bmatrix} (\gamma_1+\gamma_2)(k_x^2+k_y^2) & -\sqrt{3}[\gamma_2(k_x^2-k_y^2) - 2i\gamma_3 k_x k_y] \\ -\sqrt{3}[\gamma_2(k_x^2-k_y^2) + 2i\gamma_3 k_x k_y] & (\gamma_1-\gamma_2)(k_x^2+k_y^2) \end{bmatrix} \tag{2.5}$$

with $k_x = -i\partial/\partial x$, $k_y = -i\partial/\partial y$. The Luttinger parameters are $\gamma_1 = 5$, $\gamma_2 = 1.6$, and $\gamma_3 = 2.1$.[17] The wave function of the ground state of the valence band at $k_z = 0$ is $F_{3/2,\pm 3/2}(x,y)|\frac{3}{2} \pm \frac{3}{2}\rangle + F_{3/2,\mp 1/2}(x,y)|\frac{3}{2} \mp \frac{1}{2}\rangle$. With the above axes, where the spin quantization is parallel to the wire, $|F_{3/2,\mp 1/2}| > |F_{3/2,\pm 3/2}|$ contrary to the situation where the spin quantization is normal to the wire.[16,18] In the case of interest, the calculation shows that $|F_{3/2,\mp 1/2}| \gg |F_{3/2,\pm 3/2}|$ (about ten times larger), so that only the $|F_{3/2,\mp 1/2}|$ component is given in Fig. 2.

The calculation was carried out with $n = 0, \pm 1 \ldots \pm 12$ and $n' = 1,2 \ldots 25$. The numerical accuracy is then of the order of 1 meV.

It is important to notice that the particular case $\varepsilon = 0$ is as well described with Mathieu's equation (Sec. II B 2, parabolic bands approximation), as with the general calculation (which is numerical but takes into account the valence-band structure). However, when $\varepsilon \neq 0$, the general calculation is required since the lateral potential depends on both variables x and y, which can no longer be separated. Furthermore, in order to justify taking $V'_{Nout} = \infty$, a complete calculation was performed once using the exact finite values in the $Cd_{0.74}Mg_{0.26}Te$ barriers, namely $V'_{Cout} = 223.3$ meV and $V'_{Vout} = 111.6$ meV. This lengthy calculation gave a confinement energy that differed by less than 1 meV from the result for $V'_{Nout} = \infty$. Given the experimental and numerical accuracies, the infinite barrier approximation is thus justified.

D. Numerical results

The numerical results are presented in Fig. 1(b) (Mn TSL, various miscut angles) and Fig. 1(c) (1° miscut, TSL with Mg or Mn composition) for the energy calculation. Figure 2 gives the envelope function representations for a 1° Mn TSL.

The two main characteristics of a 1D behavior can be seen in these figures. The first one is the clear energy redshift of the ground-state emission of the TSL, about 30 meV for a 1° Mn TSL, which increases with the terrace width L_x, that is, with the wire periodicity, as can be seen in Fig. 1(b). Note

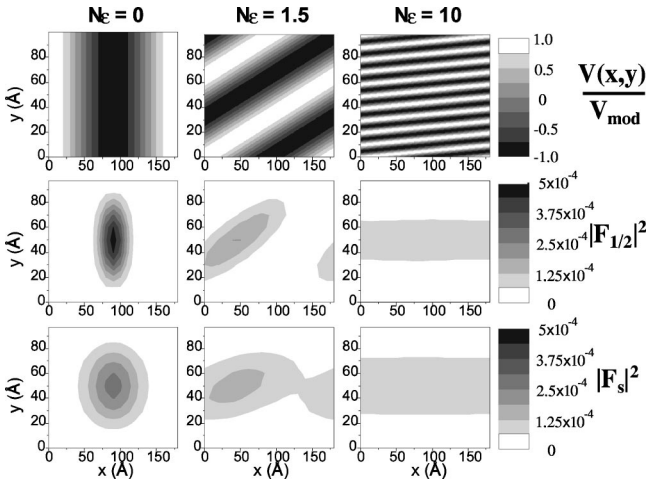

FIG. 2. Normalized modulation potential $V(x,y)/V_{mod}$ and squared modulus of electron and hole envelope functions for a 1° Mn TSL, represented versus x and y, for three different values of $N\varepsilon$, namely, 0, 1.5, and 10. The spin quantization axis is parallel to the wire. F_s represents the electron-envelope function; the hole-wave function is written $F_{3/2,\pm 3/2}(x,y)|\frac{3}{2} \pm \frac{3}{2}\rangle + F_{3/2,\mp 1/2}(x,y)|\frac{3}{2} \mp \frac{1}{2}\rangle$, but only the larger component $F_{3/2,\mp 1/2}$ is given here (see text), and written as $F_{1/2}$. The electron- and hole-envelope functions have a clear 1D behavior for $\varepsilon = 0$, and we see the evolution toward a 2D behavior when $N\varepsilon = 10$ ($\varepsilon = 0.33$); the intermediate case where $N\varepsilon = 1.5$ (i.e., $\varepsilon = 0.05$ and $\beta = 70°$) is already rather 2D-like.

also that, considering a 1° substrate, a Mg TSL gives a larger redshift (36 meV) than a Mn TSL [28 meV, see Fig. 1(c)]. The second characteristic is related to the spatial extension of the envelope functions, and can be seen in Fig. 2: the electron and hole envelope functions have a clear 1D behavior for $\varepsilon=0$, since both electron and hole are confined inside the wire. In that case, the wire section in the x direction corresponds to the dark region $x\in[45\ \text{Å};\ 135\ \text{Å}]$ of Fig. 2.

As pointed out in Ref. 12, the physical parameter that controls the confinement (1D or 2D) is $N\varepsilon$, where $N=L_y/a$ corresponds to the number of monolayers deposited while growing the TSL (N will always be equal to 30 for the superlattices studied here, see Sec. III A for more details concerning the growth). Indeed, $N\varepsilon=0$ gives a vertical superlattice, whereas when $N\varepsilon\approx1$ we begin to have more than one wire per pattern [see $V(x,y)$ in Fig. 2 when $N\varepsilon=1.5$]; in other words, the carriers can move along x as much as along y, i.e., the transition from 1D toward 2D is occurring.

Moreover, from these figures one can deduce the strong limitations on a 1D behavior, or in other words, the limiting factors that will destroy the lateral confinement. Indeed, the redshift of energy occurs in a very thin region around $\varepsilon=0$ (considering a 1° misoriented sample, $\varepsilon=0.1$ already gives a tilt angle β of around 80° as stated above, and a redshift smaller than 2 meV). This feature is also reproduced in the envelope functions (see Fig. 2): when $N\varepsilon$ goes from 0 to 10 (i.e., ε from 0 to 0.33) one can see the evolution toward a 2D behavior where both electron and hole are no longer confined in the lateral direction (x). Note that the intermediate case where $N\varepsilon=1.5$ (i.e., $\varepsilon=0.05$ and $\beta=70°$) is already rather 2D-like. Another key parameter controlling the 1D behavior is the miscut angle, or the terrace width. Indeed, for large miscut angles ($\alpha=2°$), the 1D effect is small due to the low periodicity ($L_x=93$ Å) that allows a strong coupling between adjacent wires. When the lateral periodicity gets larger (smaller miscut angles), such a coupling effect decreases, which is reflected by a larger energy redshift for the 1D behavior [see Fig. 1(b)].

However, from the experimental point of view, one has to keep in mind that the longer the terrace is, the harder it is to grow a lateral superlattice: indeed, as the terrace width increases, the adatoms have to follow a longer path in order to enable the step-flow growth mode. To grow a TSL, one must increase the growth interruption times under vacuum and/or increase the substrate growth temperature, but both conditions will also strongly increase the Cd/Mn or Cd/Mg intermixing, which tends to limit the lateral potential modulation.[13] In practice, it will thus be difficult to grow a lateral superlattice on a vicinal surface tilted less than 1°.

III. FABRICATION AND OPTICAL CHARACTERIZATION

A. Design of the samples

The growth of lateral superlattices on vicinal surfaces is based on the step-flow growth of fractional monolayers (ML's) over a very regular array of monomolecular steps. In order to fulfill the latter condition, we grow the TSL on [001] surfaces misoriented toward the [100] directions (C substrates with step edges parallel to the direction [010]). This geometry, with steps aligned along the [010] direction, is more appropriate for CdTe than the misorientation toward [110] used for growing GaAs-based TSL's, because CdTe has a natural tendency to grow with step edges aligned along [010] directions as demonstrated by scanning tunneling microscopy.[19] The growth was performed on $Cd_{0.96}Zn_{0.04}Te$ C substrates, with misoriention angles α of 1° and 0.5°, inducing terrace widths L_x of, respectively, 186 Å and 371 Å along the x direction. One can then expect to have a TSL which generates an array of wires with typical lateral sizes of about half the terrace width.

In order to fulfill the conditions for the step-flow growth mode, we chose a substrate temperature of typically 300°C, for which no oscillation of the reflection high-energy electron diffraction specular intensity is observed. This is a signature of a steady-state surface roughness, and consequently of a step-flow growth. The temperature of 300°C is adequate when the terrace width is 186 Å (misorientation of 1°). It is a compromise between a low temperature minimizing the exchange between Cd and Mn (or Mg)—which would reduce the lateral ordering[13]—and a high temperature allowing a good mobility of the adatoms, ensuring a step-flow growth. Larger terraces (smaller misorientations) require using a higher growth temperature, which generates a stronger Cd/Mn intermixing, whereas smaller terraces ($\alpha=2°$) induce smaller 1D effects due to the increasing tunneling between adjacent wires (see below and Ref. 20).

The various active layers of our samples were grown by molecular beam epitaxy (MBE). A sketch of a typical sample is shown in Fig. 3: before growing the TSL itself, we buried two quantum wells, one of pure CdTe of intended composition 25 ML (QW1), and the other one identical, but with the central CdTe ML replaced by a ML of MnTe (or MgTe) (QW2). The TSL growth then consists of depositing m ML of CdTe, followed by n ML of $Cd_{0.76}Mn_{0.24}Te$ (or $Cd_{0.74}Mg_{0.26}Te$), with m and $n\approx0.5$, this cycle being repeated $N=30$ times. As a consequence, 1° misoriented substrates give rise to approximately square wires of 93 Å $\times$97 Å.

Two kinds of samples are then obtained: Mg TSL's corresponding to an array of wires with intended composition $CdTe/Cd_{0.74}Mg_{0.26}Te$, or $CdTe/Cd_{0.76}Mn_{0.24}Te$ for Mn TSL's. The whole structure is embedded in $Cd_{0.74}Mg_{0.26}Te$ barriers, which give a large confinement in the growth direction (y), and also match the $Cd_{0.96}Zn_{0.04}Te$ vicinal substrate. Finally, our samples are at least 1 cm long, and the substrate is placed in the MBE chamber in a position where there is a marked flux gradient: this gives a TSL with a tilt angle β that varies from positive to negative values along the sample, with a vertical superlattice ($\beta=0$) at a given spot of the sample.

Such a sample design, with the two quantum wells underneath the TSL, first reported by Bloch *et al.*[20] for $GaAs/Ga_xAl_{1-x}As$, allows local evaluation of the TSL tilt angle when doing PL measurements along the sample (see Fig. 3). By exploring the sample one can find the position where the superlattice is vertical (corresponding to $p=m+n=1$, i.e., $\varepsilon=0$), as detailed in the next section.

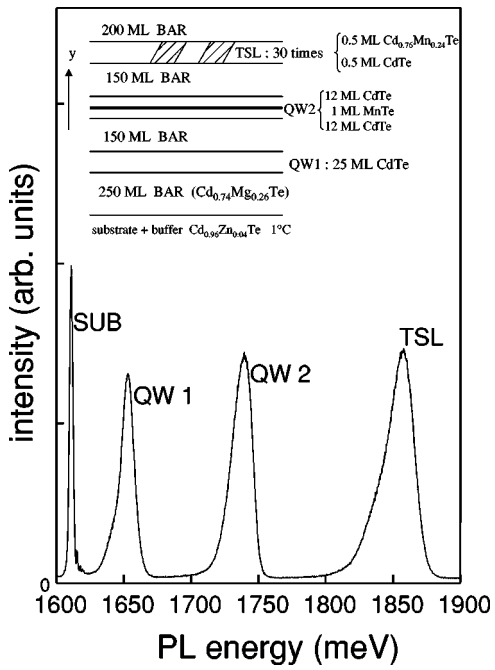

FIG. 3. Typical photoluminescence spectrum taken at 1.7 K for a Mn TSL, with sketch of the sample inserted at top. SUB denotes the substrate emission, QW1 pure CdTe quantum well, QW2 the CdTe well with one monolayer of MnTe inserted in the middle, TSL the tilted superlattice, and BAR the $Cd_xMg_{1-x}Te$ barrier. The sample's misorientation was 1°C.

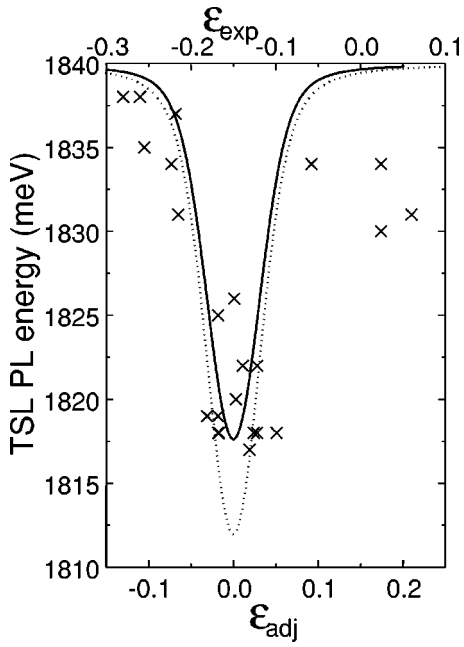

FIG. 4. Energy position of lowest emission peak of the TSL versus ε, for a Mn TSL sample. The data points ($\times$) were taken along one 1°C sample in photoluminescence experiments at 1.7 K. The dotted line corresponds to the calculation done with a value $V_{Cmod}=42.5$ meV (see text); the solid line corresponds to the theoretical calculation made with a fitted value of $V_{Cmod}=36.5$ meV. The top scale (ε_{exp}) corresponds to the value of ε calculated from the experimental spectra, whereas the bottom scale (ε_{adj}) corresponds to the value of ε adjusted in order to have $\varepsilon=0$ when the TSL is vertical.

B. cw Spectroscopy

The continuous wave experiments were performed at 1.7 K with an Ar laser. The beam diameter is about 100 μm; at this scale, any flux fluctuation can be neglected. We took spectra every 0.5 mm along each sample. A typical PL spectrum taken at a precise spot on the sample is shown in Fig. 3: this sample contained a Mn TSL, and one can clearly identify the four peaks corresponding to the substrate (labeled SUB), QW1, QW2, and TSL. Then, by plotting the TSL's PL energy versus ε (which is correlated to the CdTe flux, see below) for a given sample (see Fig. 4 for a Mn TSL), we have a fingerprint of the TSL's behavior as a function of its tilt: besides the monotonic variation due to the flux gradient along the sample, we clearly observe a superimposed redshift of up to 15 meV. The maximum redshift should correspond to the position on the sample where the TSL is vertical, as expected from the theoretical calculation described earlier (see Sec. II).

We determined the value of ε at each point of the sample as follows. The energy of a CdTe quantum-well exciton versus the well width has been calculated in Ref. 21 and enables us to deduce a precise value of *m* for the emission energy: the position of QW1 peak enables us to determine its width, and thus the precise flux of CdTe at any spot of the sample, and consequently the value of *m*. A similar analysis of the position of QW2 peak gives us the precise flux of MnTe (or MgTe) at each spot, which leads to the value of *n*. Here, we checked that whatever the dilution profile of 1 ML of MnTe (or MgTe), the energy of the ground-state exciton in a 25 ML wide well varies by only 2 meV between the two extreme cases [abrupt profile, and diffusion of all the Mn (or Mg) atoms inside the well]. Having an effective profile between these two extreme cases, the difference is small enough (2 meV) so that we can consider an abrupt profile for the evaluation of ε from the energy position of peak QW2.

Figure 4 shows the energy position of the Mn TSL's lowest energy emission versus ε, together with the calculation (dotted curve) explained earlier. The top scale (ε_{exp}) corresponds to the value of ε deduced from the spectra (see above), whereas the bottom scale (ε_{adj}) is the same scale shifted by 0.15 to adjust the minimum of emission energy in the TSL (see later). The experimental energy redshift ($\Delta E=15$ meV), which confirms the 1D character of the TSL, is smaller than the calculated one ($\Delta E=28$ meV). Two effects can explain this difference.

The first one is the exact value of the miscut angle α, i.e., the terrace width. As seen in Fig. 1(b), the larger the miscut, the smaller the expected energy redshift, due to the coupling between the wires when the periodicity gets smaller. The miscut angles of our $Cd_{0.96}Zn_{0.04}Te$ substrates were checked by x-ray diffraction and they vary from 1° up to 1.3°, so that the theoretical energy redshift ΔE could be as low as 23 meV.

The second cause for reduction of the energy redshift could be the intermixing between Cd and Mn (or Cd and Mg) that limits the lateral modulation potential V_{Nmod}. The solid line in Fig. 4, which fits the experimental data, is the

theoretical result calculated with $V_{Cmod}=36.5$ meV instead of $V_{Cmod}=42.5$ meV (dotted line).

From this value of V_{Cmod}, we can extract some new insights about the exchange between the cations in these II-VI systems. Usually, the Mn concentration profile is accounted for by assuming that exchange occurs only between the surface monolayer being grown (labeled *surf*), and the previously deposited monolayer (labeled *incorp*). Then the equilibrium can be described by a phenomenological mass action law[22]

$$\mathrm{Cd}_{surf}+\mathrm{Mn}_{incorp}\rightleftharpoons\mathrm{Cd}_{incorp}+\mathrm{Mn}_{surf}$$

with a mass action constant $K=[\mathrm{Cd}_{incorp}][\mathrm{Mn}_{surf}]/[\mathrm{Cd}_{surf}][\mathrm{Mn}_{incorp}]$. Quantitative analysis of this intermixing was done for both CdTe/Cd_xMn_{1-x}Te (Ref. 23) and CdTe/MnTe (Ref. 14) interfaces, and gave a value of $K=1$ at 280°C. We have taken this exchange into account to model the growth of the TSL on vicinal surfaces, by considering that the atoms impinging during growth are first exchanged with the most recently incorporated monolayer, and then migrate toward the step edge. With $K=1$, this approach gives a Mn composition variation along the terraces[13] between 1/3 and 2/3 of the nominal value, that is, between 8% Mn and 16% Mn instead of between pure CdTe and 24% Mn. The calculated lateral modulation potential that fits the experimental results ($V_{Cmod}=36.5$ meV) corresponds to a larger value of K ($K\approx1.2$). Because the TSL was grown at 300°C and not 280°C (in order to enable the step-flow growth mode), the exchange process described by the mass action law is expected to be thermally activated, as already shown for the Cd/Mn system at growth temperatures lower than 280°C.[14] So when the growth temperature increases above 280°C, the value of K is expected to be larger than 1, which is coherent with the experimental results.

As concerns the bottom scale of Fig. 4, it has been adjusted (shift of 0.15 between ε_{exp} and ε_{adj}) so that its origin corresponds to the minimum of emission energy observed for the TSL. This adjustment of the ε value is supported by the two following arguments: first, instead of using a square QW model in order to deduce the values of m and n, and consequently of ε, we can use a QW with segregated interfaces for the two CdTe/Cd_xMg_{1-x}Te interfaces, which leads to an estimated value of ε larger than the previous one by almost 0.1, and also does account for most of the ε shift. Second, the PL linear polarization, although it is not as strong as expected, is more pronounced for the sample area where the energy redshift is maximum: this supports our interpretation, that is the TSL sample is vertical in this considered area, i.e., ε should be equal to zero at the energy minimum.

Let us note that, in order to insure that the energy redshift is not due to a Stokes shift between the PL and the PLE, a systematic study of the TSL emission energy as a function of position was also done at higher temperature (namely, 77 K). At such temperature, the Stokes shift is expected to be smaller, but the same energy redshift is observed (with energy values shifted by the variation of the energy gap with temperature). This then justifies the results based on PL measurements, for which only the absolute values of energy have to be shifted.

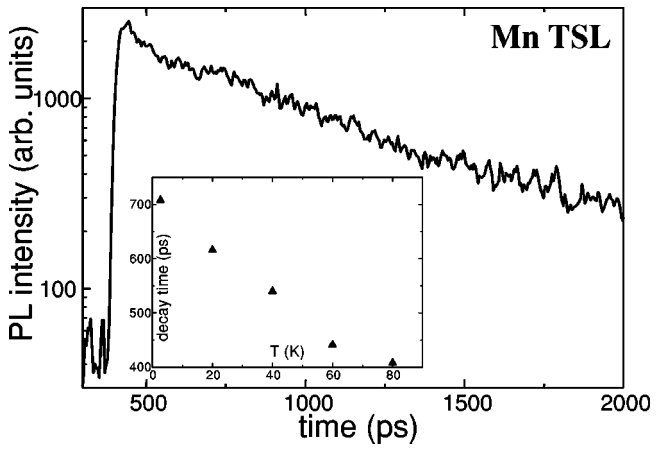

FIG. 5. Emission decay profiles from time-resolved spectroscopy for a Mn TSL sample at low temperature ($T=2.7$ K); the insert gives the evolution of the decay time versus temperature for this TSL.

IV. TIME RESOLVED SPECTROSCOPY

A. Low temperature results

Time-resolved spectroscopy experiments have been performed by exciting the CdTe/$Cd_{0.74}Mg_{0.26}$Te TSL considered above with 250 fs pulses at a wavelength of 412 nm (i.e., an energy of 3 eV). With this pumping energy, the carriers are generated in both the CdTe wires and the Cd_xMg_{1-x}Te barriers. There will be various relaxation pathways for the carriers, including the capture from reemission to the Cd_xMg_{1-x}Te barriers. In order to check that the capture time from the barriers to the TSL was not rate limiting, we have also excited below the band edges of the barriers (2.07 eV), i.e., with pumping conditions for which the carriers are directly created in the wires. Similar results are obtained in both cases, demonstrating the efficient carrier capture in these wires.

Typical decay times at low temperature, integrated over the whole energy range of each emission line, are presented in Fig. 5 for the CdTe/Cd_xMn_{1-x}Te wires, and in Figs. 6 and 7 for CdTe/Cd_xMg_{1-x}Te wires. The decay times measured at low temperature for these wires (about 700 ps for a Mn TSL, and 400 ps for a Mg TSL) are found to be systematically longer than those measured for both QW1 (pure CdTe quantum well) and QW2 (CdTe with a ML of MgTe), which are between 250 ps and 300 ps.

It is tempting to consider this as a manifestation of a TSL property, as compared to the lifetime for a QW having similar confinement dimensions, because of the finite spatial coherence of the TSL exciton in the lateral direction, which is limited by the 1D geometry. However, there are two effects that could dominate the expected effect of a longer intrinsic radiative lifetime when the exciton dimensionality decreases from 2 to 1: (i) the first one is localization of excitons in potential fluctuations due to size and alloy composition

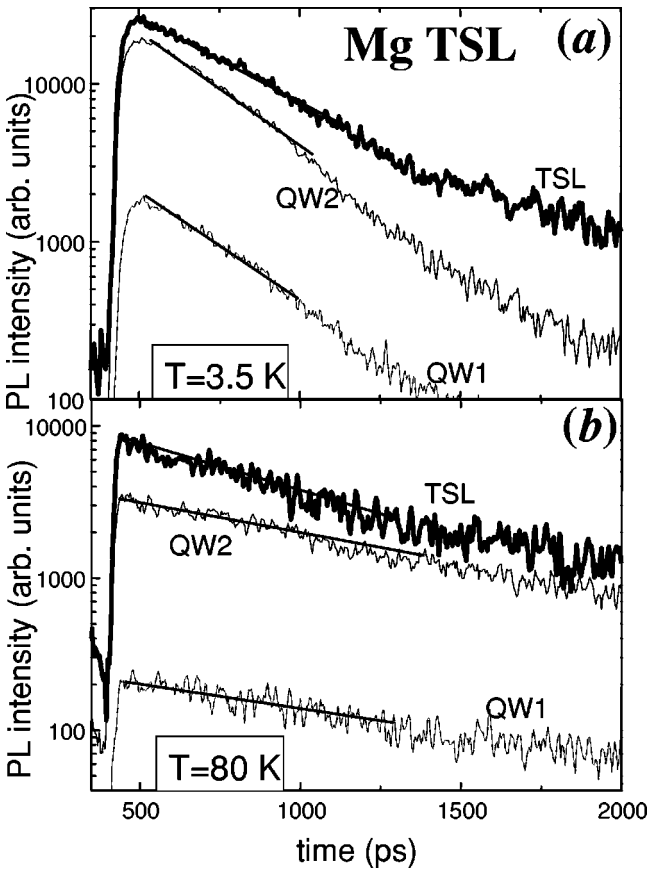

FIG. 6. (a) Emission decay profiles from time-resolved spectroscopy for QW1, QW2, and TSL, taken for a Mg TSL sample, on the area where ε is close to 0, at low temperature ($T=3.5$ K); (b) same figure at high temperature ($T=80$ K).

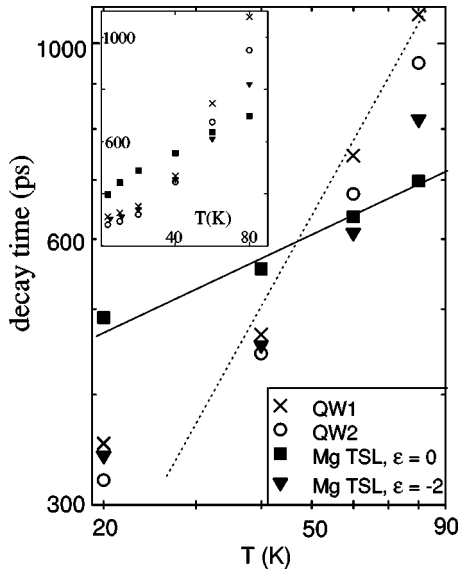

FIG. 7. Decay times versus temperature in a log scale, measured for QW1, QW2, TSL on the same spot as Fig. 5, and for the TSL on another spot where $\varepsilon \neq 0$, showing clearly the different lifetime dependence of the 1D TSL as compared to the 2D QW. The inset shows the same points on a linear scale.

variations, which also tends to increase the recombination lifetime; (ii) the second effect is the energy relaxation process, which may not be fast compared to the radiative lifetimes in one or both of the QW and TSL cases.

In order to lift the ambiguity due to these two possible effects, the temperature dependence of the PL decay time in TSL's for $T<100$ K has been studied. As pointed out by Citrin,[7] such experiments serve as an analytic tool to identify high-quality TSL's.

B. Temperature dependence

Figures 5, 6, and 7 compile decay times observed at different temperatures for exciton emission in both type of samples, $CdTe/Cd_xMn_{1-x}Te$ (Fig. 5) and $CdTe/Cd_xMg_{1-x}Te$ (Figs. 6 and 7). An increase of decay time with temperature, as observed for Mg samples, indicates that radiative recombination dominates. By contrast, in Mn samples, the decrease of the decay time versus temperature is a signature of nonradiative processes that are thermally activated and eventually dominate the recombination at high temperature: the decay time varies from 700 ps at 2.7 K to 400 ps at 80 K (Fig. 5). In these diluted magnetic semiconductor quantum wires, formation of magnetic polarons, that is a strong correlation between the carrier spins and Mn ions spins, induces a localization of the excitons at low temperature. This localization is reflected by the large exciton lifetime measured at 3.5 K (700 ps) as compared to the one measured for Mg TSL samples (400 ps), where no such localization effect exists. As temperature increases, the localization within a magnetic polaron is progressively suppressed, as already observed for QW (Ref. 24) and quantum dots.[25] The decrease of the lifetime then reflects the thermally induced redistribution of exciton population from localized states (magnetic polaron) to extended states (free excitons).

By contrast, for the Mg TSL, all PL decay times increase with temperature, and a clearly different behavior is observed between the QW and the TSL in the sample area where the superlattice is vertical. The PL decay times of the TSL are longer than those of the QW at low temperature, but shorter at 80 K (700 ps, instead of 1.1 ns for QW1). Moreover, a logarithmic scale (inset of Fig. 7) shows that the PL decay times follow a power-law temperature dependence, namely, $\tau=AT^{\sigma}$. The PL decay times of the QW increase linearly with temperature with a fitted slope $\sigma=1.2$. Similar values of the decay time τ, together with a linear temperature increase up to 80 K, have already been reported for CdTe QW's.[26]

On the other hand, for the TSL's, the temperature dependence of the decay time in the wire system (TSL $\varepsilon=0$) is fitted with a value $\sigma=0.35$. Moreover, for the part of the sample where the TSL presents a large tilt angle (TSL $\varepsilon=-2$), the PL decay time variation again increases almost linearly with temperature. This shows that, in the latter case, the TSL can be considered as a simple $Cd_xMg_{1-x}Te$ quantum well having an average Mg composition.

C. Discussion

The observed variation of the exponent σ, characterizing the power law temperature dependence, with the dimension of the system ($\sigma=1.2$ for the QW and 0.35 for the QWR) is in qualitative agreement with the theoretical model usually developed.[7,8,10,27] Due to the thermal distribution of the excitonic population within a different density of states, the exponent σ is expected to change from 1 to 1/2 when going from a 2D to a 1D system. Moreover, by comparing the experimental data with the calculations mentioned above, one can deduce (from the logarithmic scale, insert of Fig. 7) the intrinsic radiative lifetime τ_0 of the exciton at $k=0$. The averaged lifetime τ measured here is given by[27] $\tau=\tau_0\sqrt{\pi k_B T/4\Delta}$ for a 1D system, and $\tau=\tau_0 k_B T/\Delta$ for a 2D system, where $\Delta=\hbar^2 k_0^2/2M$ is the kinetic energy of excitons that can decay radiatively, with M the in-plane mass of the lowest-energy exciton. The lifetime τ_0 deduced from the experimental data is 140 ± 20 ps in the TSL, whereas it is only of the order of 1 ps in the QW. This large increase of the exciton's intrinsic radiative lifetime in QWR's by more than two orders of magnitude over that of a comparable QW can be accounted for by theory:[7] it is due to the decrease of the exciton coherence length imposed by the lateral confinement in the TSL. Let us note also that the small value of τ_0 found for a CdTe QW, as compared to lifetimes reported for GaAs QW's (10 ± 4 ps),[28] reflects the increase of the oscillator strength when going from III-V to II-VI QW's: a factor of 5 was reported for a 100 Å CdTe QW as compared to a GaAs QW with the same width.[29]

The departure of the temperature dependence of the population lifetime from the simple theoretical predictions, as observed here for both the QW ($\sigma=1.2$ instead of 1) and QWR ($\sigma=0.35$ instead of 0.5) can be due to additional contributions to the homogeneous linewidth of the exciton transition, and their temperature dependence. First there is the contribution of disorder that tends to localize the excitons, preventing them from propagating freely along the wire axis (well plane). In real heterostructures, such disorder is induced by interface roughness and composition fluctuations, which are always present, and influences the exciton population distribution (see Refs. 9 and 30 for GaAs wires, and the results presented above for Mn-based wires). A second problem could be the energy relaxation: the model for the temperature dependence assumes that excitons reach thermal equilibrium on a time scale that is fast compared to their radiative lifetime. It was predicted that this assumption could not be fulfilled in TSL's, because the bottleneck effects expected in the scattering processes can prevent rapid thermalizaton.[31,32]

Nevertheless, the temperature dependence of the PL decay time in the TSL, which is close to $T^{1/2}$, indicates the existence of rapid thermalization of excitons. Such rapid carrier relaxation (<2 ps) with no sign of the inhibited relaxation predicted for ideal 1D systems, has already been observed in fractional-layer GaAs superlattices.[33] It was proposed that in such quantum-wire array structures, the confinement potential produces high-energy states that are 2D-like, and that facilitate rapid energy relaxation. Our calculation of the electronic properties of these II-VI 1D systems confirms this interpretation (the excited states are so close to the continuum that they have rather a 2D-like behavior, whereas we can expect a 1D density of states for the lowest subband).

V. CONCLUSION

We have presented the optical properties of the lowest emission state in a tilted superlattice as a function of its tilt angle β, which is reflected by its tilt parameter ε. These II-VI TSL's, CdTe/Cd_xMn_{1-x}Te and CdTe/Cd_xMg_{1-x}Te, were grown by MBE on vicinal substrates misoriented around the (100) direction, with a lateral period of 186 Å for a miscut angle of 1°. The 1D periodic potential modulation in the TSL has been demonstrated experimentally by optical data obtained in both excitation regimes, continuous wave and time-resolved spectroscopy. In cw photoluminescence spectra, scanning of the length of the sample gives a maximum energy redshift of about 15 meV, observed at the point where the TSL is vertical. Such behavior of the emitting state in the 1D structure is accounted for quantitatively by a theoretical approach that uses a modulation potential of the form $V(x,y)=V_{mod}\cos(2\pi x/L_x-2\pi\varepsilon y/a)$ to describe the lateral confinement. This complete calculation includes the intermixing between the cations Cd and Mn (or Mg) that occurs during the growth.

In the pulsed excitation regime, the dependence of the ground-state-decay time as a function of temperature differs for the two systems. As concerns the CdTe/Cd_xMn_{1-x}Te TSL samples, a strong localization of excitons due to the formation of magnetic polarons is seen. On the other hand, for CdTe/Cd_xMg_{1-x}Te samples, the temperature dependence, which is close to $T^{1/2}$ when the TSL is vertical, demonstrates the thermal distribution of the exciton population within a 1D density of states by contrast to a 2D density. Moreover, a detailed analysis of the data allows us to evaluate the intrinsic radiative lifetime in these low-dimensional systems: the 1D radiative lifetime is found to be much longer in 1D than in 2D, due to the decrease of the exciton coherence length imposed by the lateral confinement. Moreover, the radiative lifetime of the CdTe QW is shorter than that of a GaAs QW, in agreement with the stronger oscillator strength expected for the II-VI compounds. This relative importance (interplay) between the enhancement of the oscillator strength and the exciton coherence length calls for further analysis with this II-VI material system, particularly by studying TSL and QW's of various sizes.

ACKNOWLEDGMENTS

The authors thank R. T. Cox from CEA/Grenoble for critical reading of the manuscript. This work was part of the Grenoble CNRS-CEA joint research program ''Nanophysique et Semiconducteurs.''

*Corresponding author. FAX: +33.476.885.821. Email address: lmarsal@spectro.ujf-grenoble.fr
†Present address: Institut d'Électronique Fondamentale, CNRS (UMR 6822) Université Paris Sud, F-91405 Orsay Cédex, France.

[1] P. M. Petroff, A. C. Gossard, and W. Wiegmann, Appl. Phys. Lett. **45**, 620 (1984).
[2] J. M. Gaines, P. M. Petroff, H. Kroemer, R. J. Simes, R. S. Geels, and J. H. English, J. Vac. Sci. Technol. B **6**, 1378 (1988).
[3] T. Fukui and H. Saito, J. Vac. Sci. Technol. B **6**, 1373 (1988).
[4] S. A. Chalmers, H. Kroemer, and A. C. Gossard, Appl. Phys. Lett. **57**, 1751 (1990).
[5] F. Lelarge, F. Laruelle, and B. Etienne, Europhys. Lett. **40**, 213 (1997).
[6] J. M. Hartmann, M. Charleux, J. L. Rouvière, J. Cibert, and H. Mariette, Appl. Phys. Lett. **70**, 1113 (1997); **72**, 3151 (1998).
[7] D. S. Citrin, Phys. Rev. Lett. **69**, 3393 (1992); Phys. Rev. B **47**, 3832 (1993).
[8] L. C. Andreani, F. Tassone, and F. Bassani, Solid State Commun. **77**, 641 (1991).
[9] D. Y. Oberli, M. A. Dupertuis, F. Reinhardt, and E. Kapon, Phys. Rev. B **59**, 2910 (1999).
[10] J. Feldmann, G. Peter, E. O. Göbel, P. Dawson, K. Moore, C. Foxon, and R. J. Elliott, Phys. Rev. Lett. **59**, 2337 (1987).
[11] D. Gershoni, M. Katz, W. Wegscheider, L. N. Pfeiffer, R. A. Logan, and K. West, Phys. Rev. B **50**, 8930 (1994).
[12] T. Mélin, Ph. D. thesis, École Polytechnique, France, 1998; T. Mélin and F. Laruelle, Phys. Rev. Lett. **76**, 4219 (1996).
[13] M. Charleux, J. M. Hartmann, F. Kany, D. Martrou, L. Marsal, N. Magnéa, J. L. Rouvière, and H. Mariette, Microelectron. J. **30**, 329 (1999).
[14] F. Kany, PhD thesis, Université J. Fourier, Grenoble, France, 1997; H. Mariette, F. Kany, J. M. Hartmann, and H. Ulmer-Tuffigo, Appl. Surf. Sci. **123/124**, 710 (1998).
[15] *Handbook of Mathematical Functions*, Natl. Bur. Stand. Appl. Math. Ser. No. 55, edited by M. Abramowitz and I. A. Stegun (U.S. GPO, Washington, D.C., 1964).
[16] D. Brinkmann and G. Fishman, Phys. Rev. B **56**, 15 211 (1997).
[17] These values arise from a detailed analysis of the experimental data published in Le Si Dang, G. Neu, and R. Romestain, Solid State Commun. **44**, 1187 (1982).
[18] P. C. Sarcel and K. J. Vahala, Phys. Rev. B **42**, 3690 (1990).
[19] D. Martrou, J. Eymery, P. Gentile, and N. Magnéa, J. Cryst. Growth **184/185**, 203 (1998); Phys. Rev. Lett. **83**, 2366 (1999).
[20] J. Bloch, U. Bockelmann, and F. Laruelle, Europhys. Lett. **28**, 501 (1994).
[21] Numerical resolution of the Schrödinger equation with the Runge-Kutta method, taking the binding energy of the exciton into account, see R. André, Ph. D. thesis, Université J. Fourier, Grenoble, France, 1992.
[22] J. M. Moison, C. Guille, F. Houzay, F. Barthe, and M. Van Rompay, Phys. Rev. B **40**, 6149 (1989).
[23] W. Grieshaber, A. Haury, J. Cibert, Y. Merle d'Aubigné, A. Wasiela, and J. A. Gaj, Phys. Rev. B **53**, 4891 (1996).
[24] D. R. Yakovlev, in *Festkorperprobleme/Advances in Solid State Physics*, edited by U. Roessler (Vieweg, Braunschweig, 1992), Vol. 32, p. 251.
[25] A. A. Maksimov, G. Bacher, A. McDonald, V. D. Kulakovskii, A. Forchel, C. R. Becker, G. Landwehr, and L. W. Molenkamp, Phys. Rev. B **62**, R7767 (2000).
[26] A. Polhmann, R. Hellmann, E. O. Göbel, D. R. Yakovlev, W. Ossau, A. Waag, R. N. Bicknell-Tassius, and G. Landwehr, Appl. Phys. Lett. **61**, 2929 (1992); I. Lawrence, W. W. Rühle, G. Feuillet, H. Tuffigo, H. Mariette, C. Bodin, and J. Cibert, J. Phys. IV **C5**, 405 (1993).
[27] H. Akiyama, S. Koshiba, T. Someya, K. Wada, H. Noge, Y. Nakamura, T. Inoshita, A. Shimizu, and H. Sakaki, Phys. Rev. Lett. **72**, 924 (1994).
[28] B. Deveaud, F. Clérot, N. Roy, K. Satzke, B. Sermage, and D. S. Katzer, Phys. Rev. Lett. **67**, 2355 (1991).
[29] Y. Merle d'Aubigné, H. Mariette, N. Magnéa, H. Tuffigo, R. T. Cox, G. Lentz, Le Si Dang, J. L. Pautrat, and A. Wasiela, J. Cryst. Growth **101**, 650 (1990).
[30] J. Bellessa, V. Voliotis, R. Grousson, X. L. Wang, M. Ogura, and H. Matsuhata, Phys. Rev. B **58**, 9933 (1998).
[31] H. Sakaki, Jpn. J. Appl. Phys., Part 2 **28**, L314 (1989).
[32] H. Benisty, C. M. Sotomayor-Torres, and C. Weisbuch, Phys. Rev. B **44**, 10 945 (1991).
[33] A. Chavez-Pirson, H. Ando, H. Saito, N. Kobayashi, and H. Kanbe, Appl. Phys. Lett. **69**, 218 (1996).